Three-Dimensional Velocity and Concentration Measurements and Simulations of a Scaled Jack Rabbit II Mock Urban Array

Mark Owkes[a], Michael Benson[b], Christopher Elkins[c], Nicholas Wilde[d], Bret Van Poppel[b]

[a]*Montana State University, Department of Mechanical and Industrial Engineering, Bozeman, MT, USA*
[b]*United States Military Academy, Department of Civil and Mechanical Engineering, West Point, NY, USA*
[c]*Stanford University, Department of Mechanical Engineering, Stanford, CA, USA*
[d]*Massachusetts Institute of Technology, Department of Aeronautics and Astronautics, Cambridge, MA, USA*

Abstract

Magnetic resonance (MR) techniques provide non-invasive, three-dimensional measurements of velocity and concentration fields. Applying MR techniques to measure flows of contaminants through urban arrays provides a wealth of information that is difficult to obtain with large-scale field tests. In this project, a 1:188 scaled model of the phase 1 Jack Rabbit II field test was replicated and studied using a water tunnel with properties chosen to mimic field conditions. Three-dimensional, time-averaged flow data was measured using magnetic resonance velocimetry (MRV) and magnetic resonance concentration (MRC) techniques. The scaled flow was also modeled with large-eddy simulations (LES) to provide a dataset for comparison with the MR based measurements. Despite a complex, three-dimensional flow field, both velocity and concentration show good agreement between the experimental measurements and simulation data. Measurement uncertainty was estimated to be $\pm 5\%$ of each of the measured velocity components at each location for MRV

Email addresses: mark.owkes@montana.edu (Mark Owkes), michael.benson@westpoint.edu (Michael Benson), celkins@stanford.edu (Christopher Elkins), nwilde@mit.edu (Nicholas Wilde), bret.vanpoppel@westpoint.edu (Bret Van Poppel)

and ±4% of the measured concentration at each location for MRC.

Keywords: Magnetic Resonance Concentration, Large Eddy Simulation, contaminant Dispersion

1. Introduction

Dispersion of contaminant sources in built-up environments is an active area of research for the experimental, simulation, and modeling communities. The inclusion of relatively dense contaminant gases as compared to air, such as the commonly studied toxic industrial chemicals (TICs) ammonia or chlorine in their vapor phases, can further complicate the testing and analysis. The prevalence of these two toxic industrial chemicals is widespread, with a 2011 report indicating chlorine production in the United States alone exceeded 13 million tons [17], and chemical-related accidents rank chlorine second only to carbon monoxide. Precisely because of this threat, which includes risks during manufacturing, usage, and transportation, a series of large-scale experiments were conducted by a group of U.S. Federal agencies at Dugway Proving Grounds, Utah, USA, in years 2015 and 2016, collectively known as the Jack Rabbit II trials.

The Jack Rabbit II trials have been studied and documented in several works [11, 23, 22, 15, 13, 18, 24] among many others, and fully described in the accompanying introductory paper [16]. The field tests continue to be an important dataset for simulation and modeling, and included studies related to corrosion, personal protective equipment, and other impacts to emergency responders. McKenna and co-workers used two separate integral dispersion models in their study [18], and concluded that including rainout effects improved model performance when compared to field test data. Gant and co-workers use similar methods and extended the analysis to include a dense gas dispersion model from the U.S. National Center for Atmospheric Research [11]. Vik and co-workers conducted large eddy simulations to predict dispersion in the near field in and around the urban array [24] and included droplet transport and evaporation within their study for release trial number 5, finding good agreement with field test data.

While the bulk of the works presented to date has emphasized analysis of and comparison to field test data, this work focused on the complex flow in the near field for phase 1 tests with the CONEX container mock urban array. This work removes the dense gas and phase change complexities, enabling

detailed study of a single phase dispersion event. This simpler study was conducted using a scaled version of the field test geometry within a water tunnel that maintains the geometrical complexity of the Jack Rabbit II field tests.

The experiment used Magnetic Resonance (MR) measurements of the three-dimensional velocity field and contaminant. The MR datasets provide non-intrusive, three-dimensional measurements at a high spatial resolution of 0.8 mm (compared to the channel cross-section of 196×110 mm). Along with laboratory control and measurement of inflow conditions for both contaminant injection and freestream atmospheric flow, the measurements provide a dataset for comparison with the field study, reduced-order models, and simulations.

The measured inlet boundary condition and steady flow characteristics of the experimental work provide excellent validation data for simulation efforts. Once validated, model enhancements that incorporate the additional complexity of the field test data should perform more accurately. In addition, the number of measurements within the dataset – with literally millions of measurement locations with three velocity components and concentration – provide an unprecedented opportunity for comparisons. Indeed, existing metrics for comparisons will need to be expanded to leverage the full extent of the available data, with several proposed in this study. We match the geometrical complexity of the Jack Rabit II field tests but not the atmospheric conditions such as the chlorine phase change and interaction with the atmosphere.

A large eddy simulation (LES) was conducted for initial comparisons with the experimental work to demonstrate the MR measurements agree with high-fidelity simulations. The LES simulations were setup to mimic the MR experiment and used the same geometry of the water tunnel, buildings, and roughness area. The fluid density, viscosity, and flow rates were matched. An inflow velocity profile, measured with MR, was used as the upstream boundary condition. The LES includes a number of parameters and in this study we chose to use the default values with the goal of comparing results from the two methods. In this work, *no* effort was made to improve the LES results by adjusting model parameters. Future work will include improving the simulation parameters to best match MR results.

2. Methods

2.1. Jack Rabbit II Trial

The Jack Rabbit II experiment consisted of many trials. Throughout the Jack Rabbit II field study, measurements were taken of the concentration and meteorological data, including wind direction and speed, humidity, and temperature. This work studied a scaled version of trial 5, chosen for its high chlorine mass released and favorable atmospheric conditions during the test. Additionally, trial 5 was determined to have the most quasi-steady release condition, a consistent wind speed and direction, and a relatively long and continuous release of contaminant. Since the MR experimental technique implemented in this study employed constant inflow conditions and a continuous contaminant release, trial 5 was the case most replicable in the laboratory.

2.2. Overview of Scaled Urban Array

The MR experiments and associated LES simulations were conducted with a scaled-down replica of the grid of the CONEX container mock urban array used in the field experiments. The scaled test section is placed within a water tunnel as shown in Figure 1, which contains a 5.08 cm diameter inlet that flows into a diffuser and honeycomb section to slow the flow and improve flow uniformity. The uniform flow passes over a roughness section that creates a boundary layer to mimic the atmospheric boundary layer in the field experiment. The roughness section contains cylinders that are 1.83 mm tall with diameters of 4.8 mm. The cylinders are organized in a grid aligned with the flow channel with 7.87 mm center-to-center spacing. The conditioned flow then passes over the test section, shown in Figure 2, and finally exits through the outlet. The test section is a 1:188 scaled section of the field experiment urban array. All the buildings are 13 mm tall except one that is 39 mm tall. The front half of the array is geometrically similar to the chlorine-based experiments, while the latter half incorporates a few subtle changes designed for comparison with sonic anemometry tests that occurred several months later. This size was chosen to balance the fraction of the scaled urban array that fit within the water tunnel and the size of the urban array buildings. The experimental flow channel components were 3D printed using stereolithography (SLA) additive manufacturing techniques with Accura 60 resin [2]. This material was chosen because 1) it is nearly

transparent, which allows optical viewing of the contaminant, and 2) is non-ferrous, a requirement for all materials used in an MR experiment.

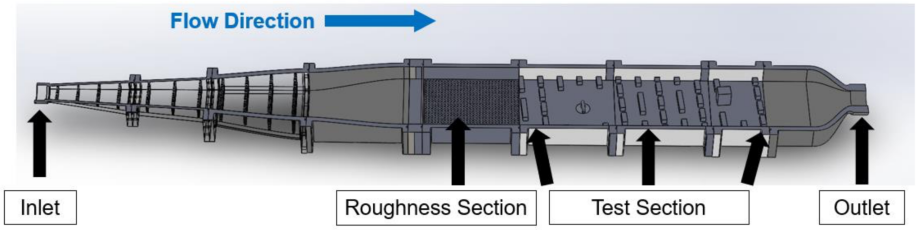

Figure 1: Sketch of water tunnel used for experiments, highlighting key components and flow direction.

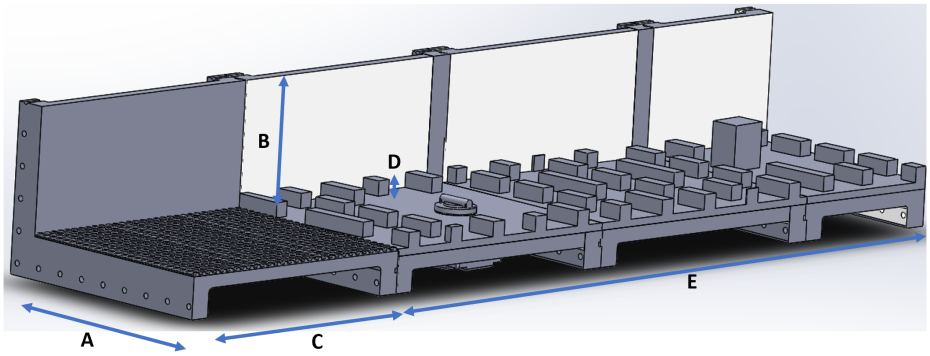

Label	Description	Dimension
A	Internal Channel Width	196 mm
B	Internal Channel Height	110 mm
C	Roughness Section Length	237 mm
D	Standard Building Height	13 mm
E	Mock Urban Array Length	609 mm

Figure 2: Cut out of geometry including the roughness section and mock urban array test section used for experiments along with dimensions.

During trial 5 of the Jack Rabbit II experiment, the wind was not directly inline with the CONEX container array. On average the wind was measured to be 4.5° from the array centerline [12]. To account for this fact, the scaled urban array was rotated relative to the water tunnel by 4.5° degrees. This can be seen in Figure 2, as the rows of buildings in the test section are not

perpendicular to the water tunnel. Furthermore, Figure 3 shows the location of the section of the CONEX array within the water tunnel along with the MR measurement areas.

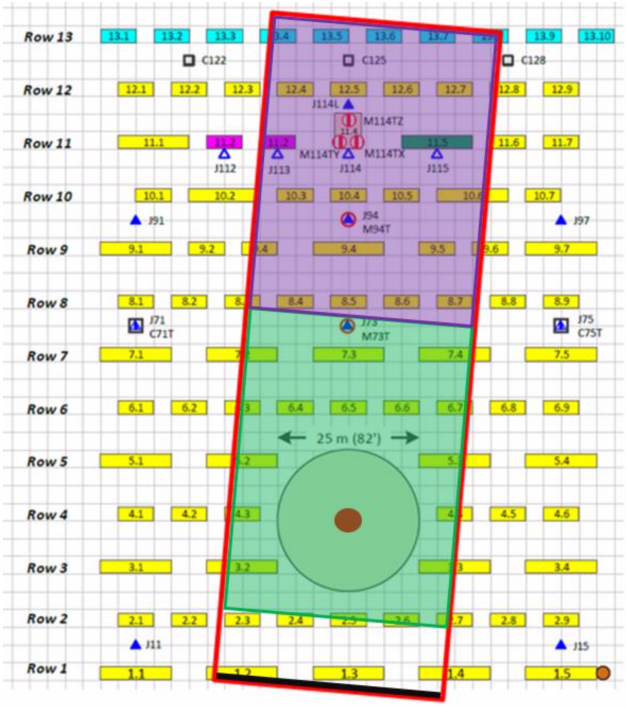

Figure 3: Overhead view of the CONEX container array used in Jack Rabbit II field test (yellow squares), portion of the CONEX container array within the water tunnel (red boundary), Chlorine release point (red circle), MRC scan region (green shaded region), and MRV scan region (green and purple shaded regions).

Contaminant was injected to replicate the release from the storage tank used in the Jack Rabbit II experiments. Note that the release in the laboratory experiment differs from the JRII experiment in that the release was not denser than the ambient flow. Figure 4 shows the contaminant injection assembly that bolts to the bottom of the test section. The storage tank measures 7.3 mm in diameter and is 30 mm in length. Due to the scale of the cylinder in the test section and the required flow rate of the contaminant, it was not possible to inject from the cylinder. Instead, contaminant was injected from the bottom of the test section. Contaminant flow enters the injector geometry through a 90° elbow, travels vertically through a short pipe and contraction, and impinges on a splash plate that is 35.25 mm in

diameter. The flow is forced radially outward through a 1 mm tall gap. The gap is small to generate a radial velocity great enough to prevent the main channel flow from entering the gap and mixing with the contaminant before it exits the gap. The radial flow penetrates upstream about 5 mm, where a stagnation point exists. The radial out flow is meant to mimic the flow out of the bottom of the cylindrical chlorine tank which impinged on the ground and then turned radially in all directions.

The Reynolds number of the flow was 44,000 based on the channel hydraulic diameter. Previous work using the same water channel with a different test section suggested that the fully turbulent flow provides a reasonable comparison with full scale atmospheric tests, as reported in [4].

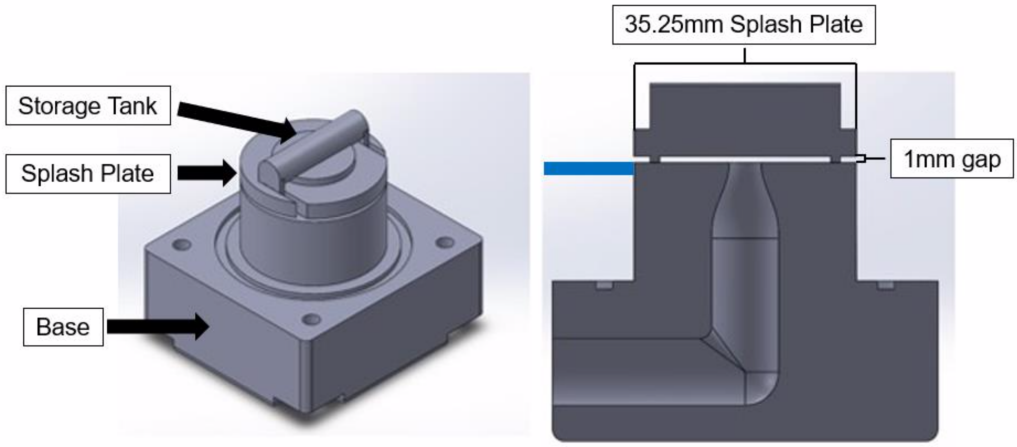

Figure 4: Isometric view (left) and cross section (right) of the contaminant injection assembly that mimics the release from a storage tank. Contaminant flows through the base, strikes the splash plate, and moves radially outward through the gap between the splash plate and the test section floor (blue).

2.3. Magnetic Resonance Fundamentals

The measurements of velocity and passive contaminant concentration in this study were based on the MRV and MRC techniques described by Elkins and Alley [10] and Benson and co-workers [5], respectively. These techniques have been applied to study the flow of a contaminant within a mock Oklahoma City model [4].

Both techniques produce three-dimensional, time-averaged datasets. Common Magnetic Resonance Imaging (MRI) systems used for medical imaging

measure the signals from hydrogen protons, leveraging the principle that hydrogen protons in water subjected to a strong magnetic field precess about that field with the Larmor frequency which is proportional to the local magnetic field strength. Magnetic resonance imaging systems manipulate the protons using radio frequency pulses and spatially and temporally varying magnetic field gradients to encode many different types of information in the proton signals. While water is the working fluid in most tests, a contrast agent–copper sulfate in the work reported here–is often added to enhance the signal and improve the signal-to-noise ratio. The MRV sequences manipulate phase and frequency to make the signals sensitive to proton motion. The MRC technique is sensitive to the chemical environment surrounding the protons. Through multiple excitations and signal acquisitions over several seconds or minutes, respectively, a two-dimensional or three-dimensional array of data can be constructed. As such, each data array represents a time average over multiple flow-through times even for the largest turbulent structures. Aside from noise, multiple two-dimensional and three-dimensional images compare well to each other, further corroborating the quality of MR methods.

2.4. Experimental Methods

The experiments were performed at the Richard M. Lucas Center for Magnetic Resonance Imaging and Spectroscopy at Stanford University using a 3.0 Tesla GE Healthcare Discovery 750 MRI system. Figure 5 shows a schematic of the experimental setup. For the MRV measurements, a 0.06 M aqueous copper sulfate solution was used for both the main and injected flows. From one large reservoir, the flow has two paths. The first uses parallel pumps to create a flow rate of 410 ± 2 L/min that enters through the main channel inlet. The other uses a single pump to generate a flow rate of 1.2 ± 0.05 L/min through the injector shown in Figure 4. To maintain constant fluid temperature and viscosity, a heat exchanger was placed inside the copper sulfate tank and connected to the building chilled water line.

The MRC experimental setup required several additional elements. In this experiment, the working fluid was water, while the contaminant was a copper sulfate solution. To reduce the effects of overall contamination of the water, a large tank farm was included in the design, comprising six inter-connected 275 gallon (1041 liter) tanks. Water from these tanks was pumped in and out of the large water reservoir in the magnet room. MRC measurements required at least three different types of scans in order to

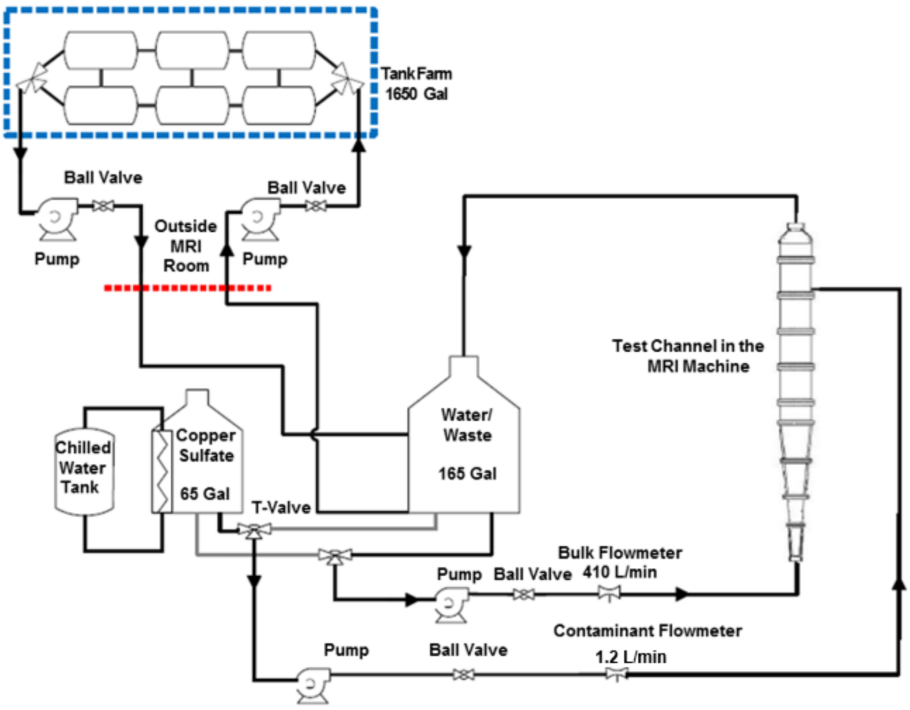

Figure 5: Schematic of experimental setup, highlighting test section, contaminant flow loop, and supporting tank farm (external and adjacent to test facility).

capture the mixed concentration field: reference conditions which use 0.02 M aqueous copper sulfate solution pumped through both the main channel and injector; background conditions which use water in the channel and injector; and standard conditions which use water in the channel and copper sulfate in the injector. To supply these fluids to both the channel and injector, the complicated plumbing setup illustrated in Figure 5 was required. An additional "standard-high" condition was measured with a 0.1 M solution for the injected fluid. By increasing the concentration of the solution, the injected fluid can be tracked farther downstream.

As shown in Figure 3, the three-dimensional, time-averaged, three component velocity fields in two overlapping regions of the mock urban array were measured using MRV. The upstream measurement volume surrounded the injector and three rows of CONEXs downstream. This volume was 26.5 cm in the flow direction, 21.2 cm in width, and 12.8 cm in height. The measurement matrix was 320 by 256 by 160 and each scan lasted 10 minutes and

37 seconds. The MR acquisition technique measures within discrete volumes throughout the field of view that are 0.8 mm per side in x, y, and z directions. The resulting volumetric element – termed voxel – is nominally 0.512 mm^3 and produces a measurement from the signals of the hydrogen protons within that voxel. A total of 11 flow on and 7 flow off scans were combined and averaged to produce the time-averaged velocity field. The average of the preceding and succeeding flow-off scans were subtracted from the average of each set of flow on scans to correct for eddy currents and system drift. The downstream measurement volume was 25.6 cm in the flow direction, 21.0 cm in width, and 123.2 cm in height with a corresponding measurement matrix of 320 by 262 by 154. Each scan required 10 minutes and 44 seconds to complete, with 10 flow on and six flow off scans combined and averaged to produce the time-averaged velocity field. The scan time is a physical run time during which the scanner acquires a full dataset in frequency space. The duration is long enough to achieve steady flow conditions and much longer than relevant flow time scales. After averaging the flow on and flow off scans, the data were processed using the divergence free filter described in Schiavazzi and co-workers [21] to produce the final velocity datasets.

The uncertainty in the velocity field measurements were calculated to be $\pm 5\%$ of the reported value as a conservative maximum and included both statistical variations on a point-by-point basis throughout the measurement domain and bias errors incurred by flowmeters and temperature probes used to maintain constant flow conditions. The velocity uncertainty varies spatially. In most regions of the flow, the uncertainty was substantially less than $\pm 5\%$; however, in regions near solid surfaces the reported value for uncertainty is more representative.

An inlet velocity profile of the flow as it enters the mock urban array test section was created from MRV measurements. This plane of data is useful for providing inlet velocities for CFD simulations. For the inlet flow, the time-averaged three-component velocity field was measured in a two-dimensional plane a distance of three building heights upstream of the test section's leading edge. The measurement plane was 24 cm wide and 14.4 cm high with an imaging matrix of 300 by 180 and slice thickness of 3 mm. A total of 80 two-dimensional scans were sampled for both flow on and flow off, all of which were combined and averaged.

The MRC experiments were conducted according to the methods described by Benson et al. [5] with extended dynamic range using a high molarity copper sulfate solution as employed by Yapa et al. [25]. The scan

volume was 26.5 cm in the flow direction, 21.2 cm in width, and 13.44 cm in height. The measurement matrix was 320 by 256 by 168, and each scan required 4 minutes and 37 seconds. In total, 16 reference, 10 background, and 14 standard scans were combined using the equation

$$C(x,y,z) = \frac{\langle STD(x,y,z)\rangle - \langle BAK(x,y,z)\rangle}{\langle REF(x,y,z)\rangle - \langle BAK(x,y,z)\rangle} \tag{1}$$

to produce the mean local scalar concentration. The $\langle\cdot\rangle$ operator denotes the mean signal magnitude array for each type of scan: STD has a copper sulfate solution (0.02 M) injected into the mainstream water flow; BAK has water in both the main and injector flows; and REF has copper sulfate solution (0.02 M) in both the main and injector flows. In addition, 19 high concentration standard (STDHI, 1.0 M) scans were completed. A similar formula to Eq. 1 was used to produce a concentration field (CHI) with better accuracy for concentrations below 0.10. The STD and STDHI cases were blended together in the following way: C was used for concentrations above 0.18; C and CHI were averaged for concentrations between 0.12 and 0.18; and CHI was used for concentrations below 0.12. The final three-dimensional concentration field was estimated to have ±4% uncertainty based on a 95% confidence interval. The uncertainty in the concentration measurements was obtained in a manner similar to that reported for the MRV. The bias errors of flowmeters and fluid temperature measurement devices were combined with the statistical uncertainty of the Standard cases for a point-by-point uncertainty estimate. When the standard high cases were included, the resulting uncertainty decreased. This result was attributable to the ability to measure to a lower concentration threshold, and the algorithm itself which used only the standard high data for regions of the lowest measured concentrations.

2.5. Simulations Methods

Large eddy simulations were performed on a subset of the geometry used for the water tunnel experiments. The LES simulations employed a truncated inflow region that started within the roughness section. At this location, mean streamwise velocity measurements taken with the MRV technique were used as the inflow boundary condition for the LES simulations. The mean velocity was perturbed with a 10% turbulent fluctuation. The LES simulations employed a simplified outflow geometry. Besides the truncated geometry, the geometry of the water tunnel, buildings, and roughness area

matched the MR experiments. Furthermore, fluid properties and flow rates (and thus Reynolds numbers) were matched between the LES and MR experiment.

The LES simulation was performed with the Star-CCM+ version 12.04.-011 [1]. The Navier-Stokes equations were solved with an implicit unsteady formulation with constant fluid density. The sub-grid turbulence was represented with the WALE sub-grid scale LES model with a $y+$ wall treatment [19]. The contaminant was modeled as a passive scalar convected with the flow and diffusing with a turbulent diffusion model based on a Schmidt number of 0.9 [9]. LES provides time dependent solutions of the Navier-Stokes equations. To compare with the MR results, which are time average measurements of contaminant concentration and velocity, the LES solution needs to be averaged in time. The averaging was performed by running the simulation until steady state was reached – three flow through times defined with the bulk channel flow and the length of the test section. The steady state flow was then averaged over a time of one flow through time.

Simulations were performed on three different mesh resolutions to assess mesh sensitivity. The coarse, medium, and fine meshes included 0.5 million, 4.6 million, 10.2 million grid cells, respectively. The medium mesh provides a maximum $y+$ of 1.2 indicating reasonable resolution of the walls [20] and a mesh that will provide converged results. This was confirmed by comparing the results at different mesh resolutions. Figure 6 shows a comparison of the streamwise velocity profile through the CONEX container array. Even on the coarsest mesh, the velocity was reasonable and matched most of the flow characteristics from simulations on finer meshes. The results from the medium and fine simulations have the same large scale features, with a few additional small-scale structures visible on the fine mesh. Figure 7 compares iso-surfaces of a contaminant concentration of 0.075. While there is a significant difference between the coarse and medium meshes, the results from the medium and fine simulations predict upstream penetration of the contaminant to roughly the same location. Furthermore, the medium and fine simulations predict the plume at a concentration of 0.075 to extend to the first full row of buildings downstream of the injector indicating the the contaminant dispersion is predicted at the same rate. These results all suggest that the medium mesh provides a mesh converged solution.

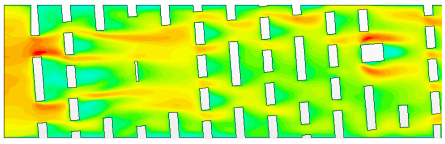

(a) Coarse Mesh

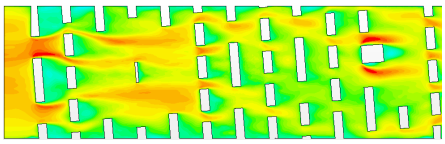

(b) Medium Mesh

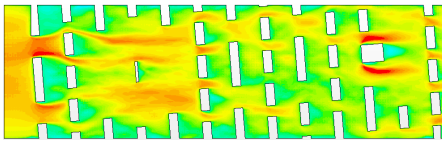

(c) Fine Mesh

Figure 6: Contour plots of streamwise velocity, V_z, from LES simulations on different meshes.

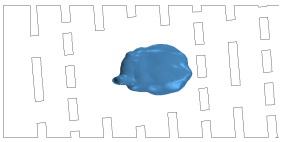

(a) Coarse Mesh

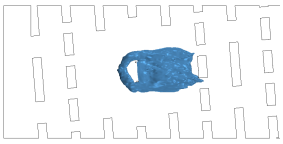

(b) Medium Mesh

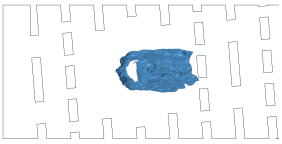

(c) Fine Mesh

Figure 7: Isosurface of contaminant at a concentration of 0.075 from LES simulations on different meshes.

3. Results

In this section, the MR measurements and LES predictions are described. For these results, the x, y, and z axes correspond to the streamwise, spanwise, and vertical directions, respectively. All velocities are scaled by the reference velocity $U_{ref} = 0.31$ m/s, which is the average streamwise velocity before the building section, and concentrations are reported on a non-dimensional scale between zero and one, with zero indicating no contaminant and one indicating maximum concentration, which occurs at the source.

3.1. Velocity Results

The MRV technique allows for three-dimensional measurements of the mean three-component velocity field. The technique has been applied to a range of applications including [6, 10, 7, 3, 8]. These works have validated the MRV technique and in this section we compare the MRV measurements and LES velocity results.

Figure 8 shows a contour plot of streamwise velocity data at $z/h = 0.9$, where h is the height of a standard CONEX, 13 mm. Both the simulation and

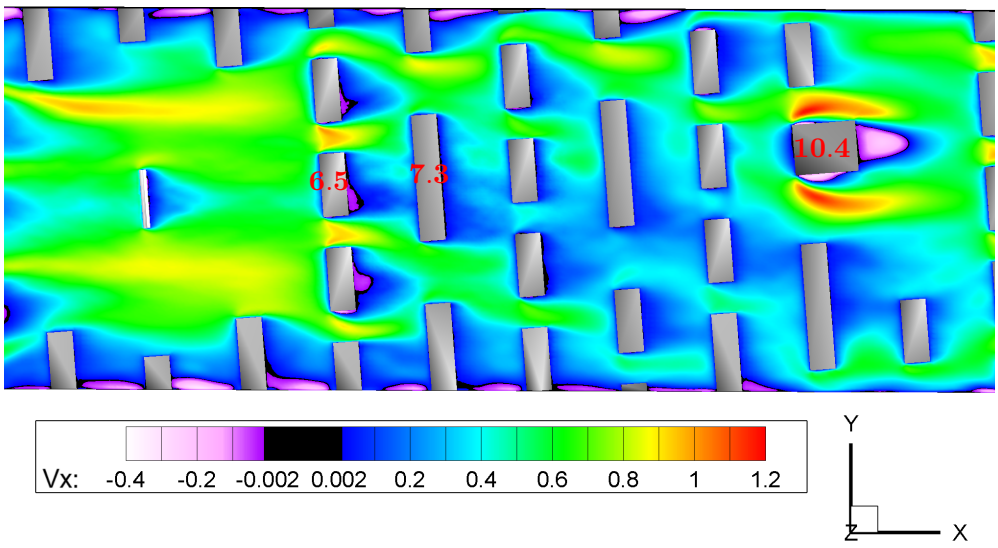

(a) LES Prediction.

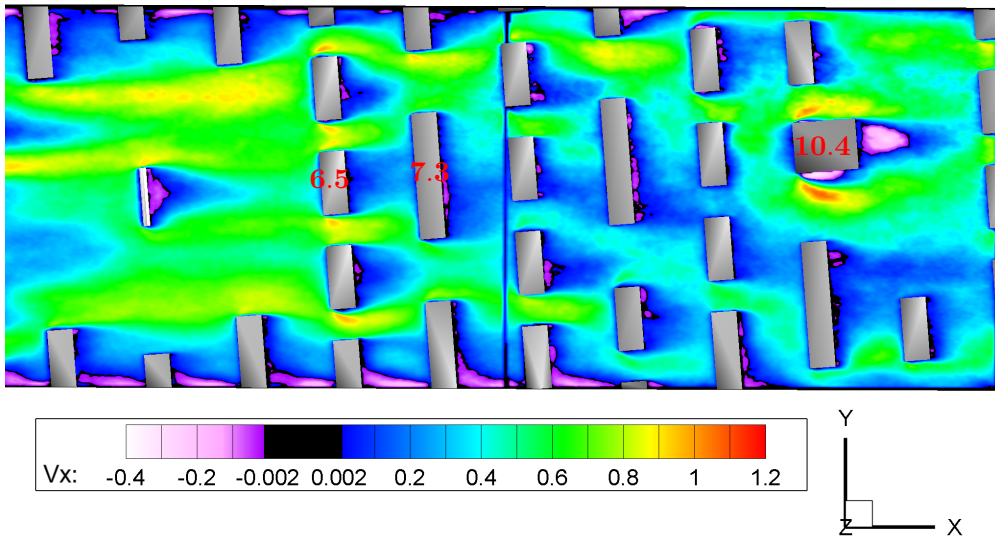

(b) MRV Measurement.

Figure 8: Streamwise velocity, V_x, from the LES (top) and MRV (bottom) on a cut plane at a height of $z/h = 0.9$. Three buildings of interest labeled in each figure.

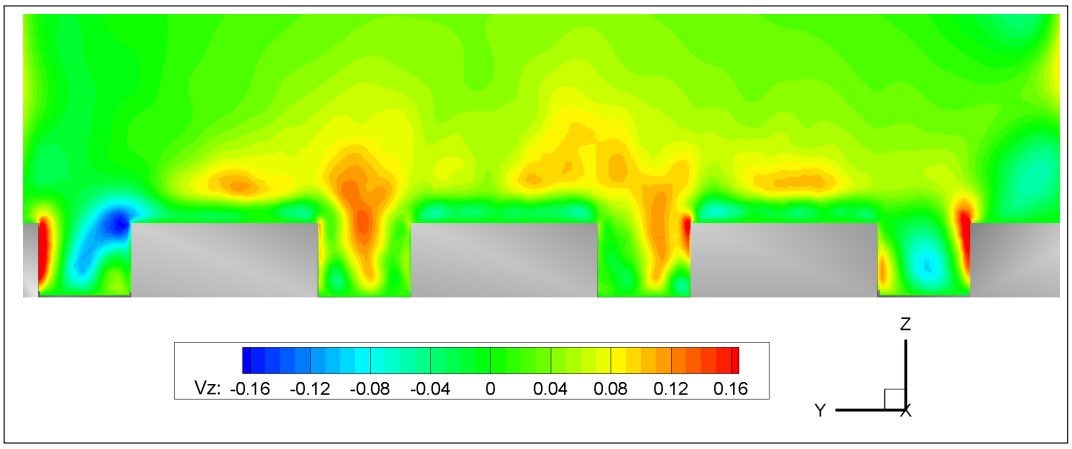

(a) LES Prediction.

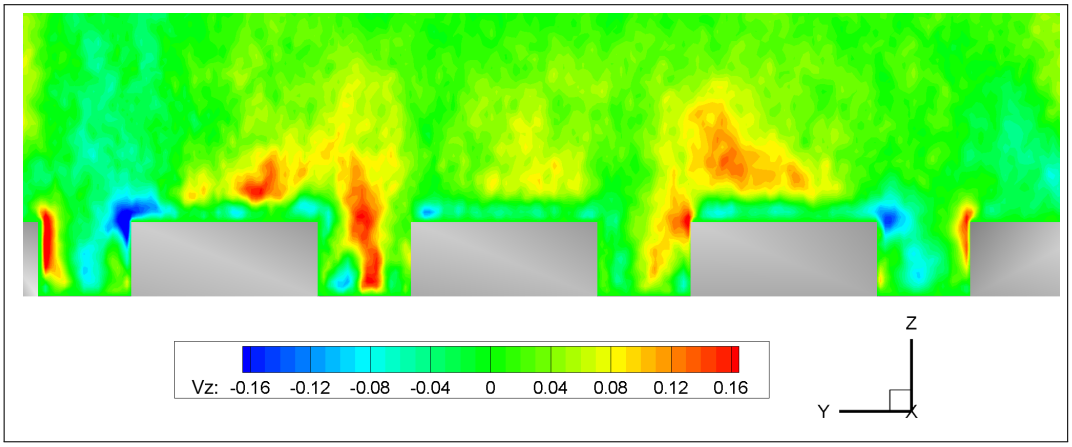

(b) MRV Measurement.

Figure 9: Vertical velocity, V_z, contours for LES (top) and MRV (bottom) looking downstream at the end of row 6, which is the first row downstream of the injector.

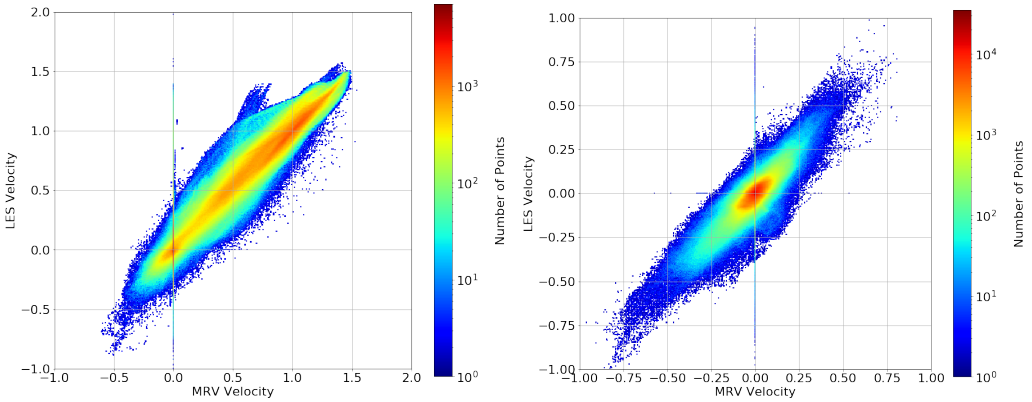

(a) Streamwise (V_x).

(b) Spanwise (V_y).

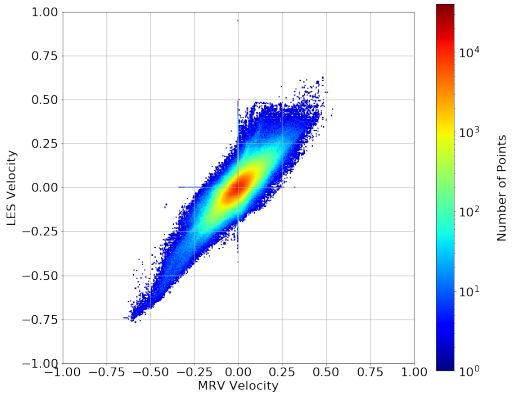

(c) Vertical (V_z).

Figure 10: Point-wise comparison of MRV measurements and LES predictions of velocity components.

experiment show a non-trivial flow field within the CONEX container array with large velocities between buildings and stagnation zones in front of and behind buildings. The inlet is asymmetric resulting in similarly asymmetric stagnation regions due in part to the 4.5° incident flow angle. Evidence of wall effects can be observed as recirculation regions near the top and bottom of the figures for both LES and MRV. The magnitude of the streamwise velocity compares very well between experiment and simulation.

There are subtle differences near a few buildings, identified by close inspection of Figures 8b and 8a. In the upstream field, building 6.5 shows greater asymmetry in the stagnation region downstream of the building for the LES, while MRV results appear to be uniform. Similar results can be observed for building 7.3 just downstream of building 6.5, with greater asymmetry in flow behind this building for LES than for MRV results. In the downstream field in the vicinity of building 10.4, flow contours show reverse flow downstream of this building for both LES and MRV, a result attributable to building 10.4 being much taller than others within the domain. The LES results show greater flow acceleration on both sides of building 10.4 than seen in the MRV results.

Figure 9 illustrates vertical velocity, V_z, contours for LES (left) and MRV (right) looking downstream at the end of row 6, which is the first row downstream of the injector. The flow after a single CONEX row has regions of vertical transport moving away from the surface on either side of the central building, towards the surface near the outside, and is asymmetric. Both MRV and LES results reveal a complex flow field with notable velocity gradients at building corners.

Figure 10 depicts a quantitative comparison of nearly 7.3 million MRV data points and LES results, using a series of point-wise scatter plots for each velocity component, with Figure 10a depicting the streamwise velocity, Figure 10b the spanwise component, and Figure 10c the vertical. Generally, MRV and LES results compare very well for all components, with a dense locus of points at or near the line $y = x$ representing perfect correlation. Some deviation can be observed in V_x at higher streamwise velocities, shown in Figure 10a in the upper right quadrant. These deviations can be traced to the wake at either side of the large building.

There is also a line of points along MRV = 0, and to a lesser degree along LES = 0. Because the MRV data was collected by scanning two separate regions, a seam is formed between the two (visible in Figure 8b). MRV measurements at this seam are all equal or nearly equal to 0, whereas they hold

a value for the LES data. Points along LES = 0 are spatially concentrated at the edge of one of the downstream buildings. Manufacturing tolerances likely led to differences between the experimental and computational geometry for this one building. There are fewer than 100 of these LES = 0 outlier points, however, accounting for about 0.001% of the data. All other differences between MRV and LES appear to be randomly distributed across the test region.

Quantitative performance metrics were calculated for each component of velocity and are tabulated in Table 1. A least squares regression yields a correlation coefficient, R, coefficient of determination, R^2, and slope of the best fit line. The fraction of points within a factor of 2 (FAC2) satisfies the acceptance criteria FAC2 $\geq$ 0.3 proposed by Hanna and Chang [14]. The fraction of LES points within MRC's 95% confidence interval (CONF95) and the hit rate, or fraction of points that satisfy either FAC2 and/or CONF95, are also reported.

Table 1: Performance Metrics for Velocity

Component	Streamwise	Spanwise	Vertical
R	0.968	0.835	0.797
R^2	0.937	0.635	0.697
Slope	0.994	0.924	0.902
FAC2	0.915	0.496	0.479
CONF95	0.390	0.750	0.789
Hit rate	0.921	0.882	0.896

3.2. Contaminant Results

One of the goals of the Jack Rabbit II studies was to investigate how contaminants move through urban arrays. The detailed experimental results measured by the MRC technique are compared in this section to the LES results to describe the dispersion features within the urban array and to address the capabilities and challenges of these advanced simulations. While the concentration results presented herein do not incorporate the complexities of the chlorine release – such as the effects of large gradients in density, phase changes, rain out, and others – they do represent laboratory-controlled single phase measurements with well-posed boundary conditions that may provide utility in assessing the performance of simulations. Furthermore, the detailed

data collected in this work are used to quantify the similarities and differences between the measured and simulated results.

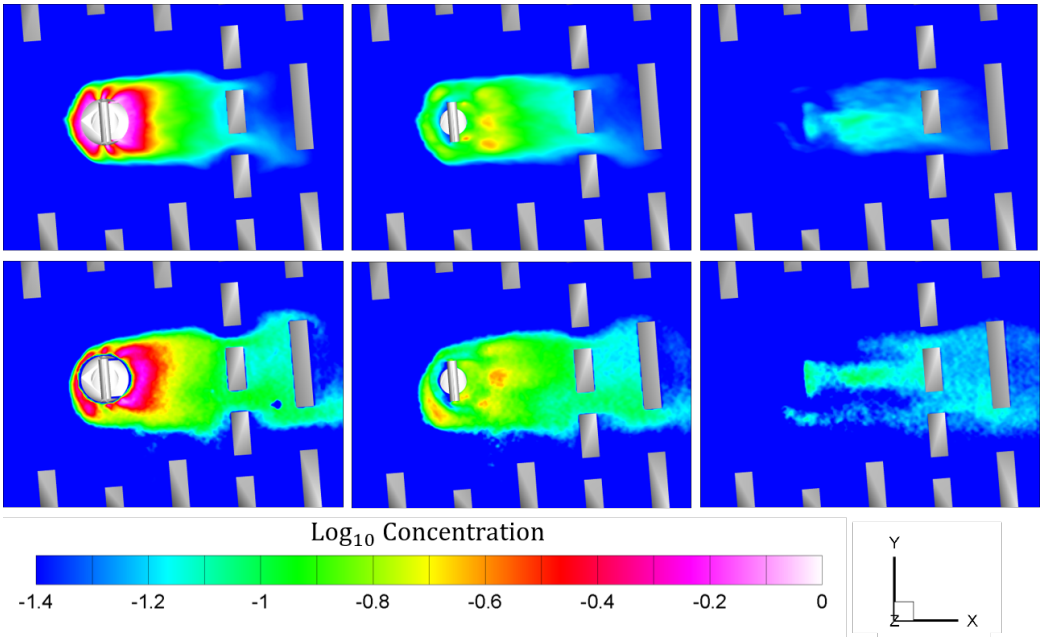

Figure 11: Concentration contours for LES (top) and MRC (bottom) at $z/h = 0.05$, 0.5, and 1.0 above bottom surface of the water tunnel.

In Figure 11, three comparisons of vertical contours are depicted for both the LES and MRC results with a logarithmic color scale. The results compare qualitatively well for the area near the injection site and up through the first buildings downstream, but the region between the final two rows of buildings compare less well. The MRC measurements in each case show a higher concentration in this building wake region, indicative of mixing in the recirculation region on the lee side, whereas the LES results imply the contaminant is transported above the building with little entrainment at the levels at or below the building height. The rate of concentration decay is overall similar, and in each case the flow around the model tank supports provides three local regions of higher concentration immediately downstream of the release at the $z/h = 0.5$ position. Even though this work employed LES simulations performed with default values, the results in Figure 11 suggest that the value of the Schmidt number used in the LES simulation was too low, thereby leading to excessive diffusion of the contaminant in sim-

ulation results. This observation highlights the potential of the detailed, three-dimensional MR datasets to inform simulations or models.

Figure 12 provides a three-dimensional view of the contaminant plume by way of concentration isosurfaces at three levels for both the LES (top) and MRC results. In each case, the isosurfaces are colored by the z-value, indicative of the plume height. The plume has its highest elevation downstream of the center of the chlorine storage tank just above the height of the buildings, with a relatively even lateral distribution to each side of the streamwise centerplane as a result of the radial release of the contaminant. The plume shape and height are matched until the interaction with the first building downstream of the injector, where the results diverge. At the lowest concentration isosurface the plume widths are still similar, but the plume elevations indicate that the LES results have more contaminant above the building height level than in the MRC.

Table 2: Performance Metrics for Concentration.

	Target Value	Calculated Value
FB	≤ 0.67	0.204
NMSE	≤ 6	0.260
NAD	≤ 0.5	0.168
FAC2	≥ 0.3	0.948
MG	1	0.739
VG	1	1.370
R	1	0.635
R^2	1	0.403
Slope	1	0.797
CONF95	1	0.754
Hit rate	1	0.948

Figure 13 depicts a quantitative comparison of the LES and the MRC results at several million data points within the plume. Visually, a perfect correlation would result in a distribution along the line $y = x$. In this comparison, the bulk of the points are close to this notional line, but there are some noteworthy variations. Overall, the MRC results tend to indicate slightly higher concentrations in some locations. The locations where these differences exist are suggestive for the reason they vary. The bulk of the points that do not match are near the edges of the injection and at the plume

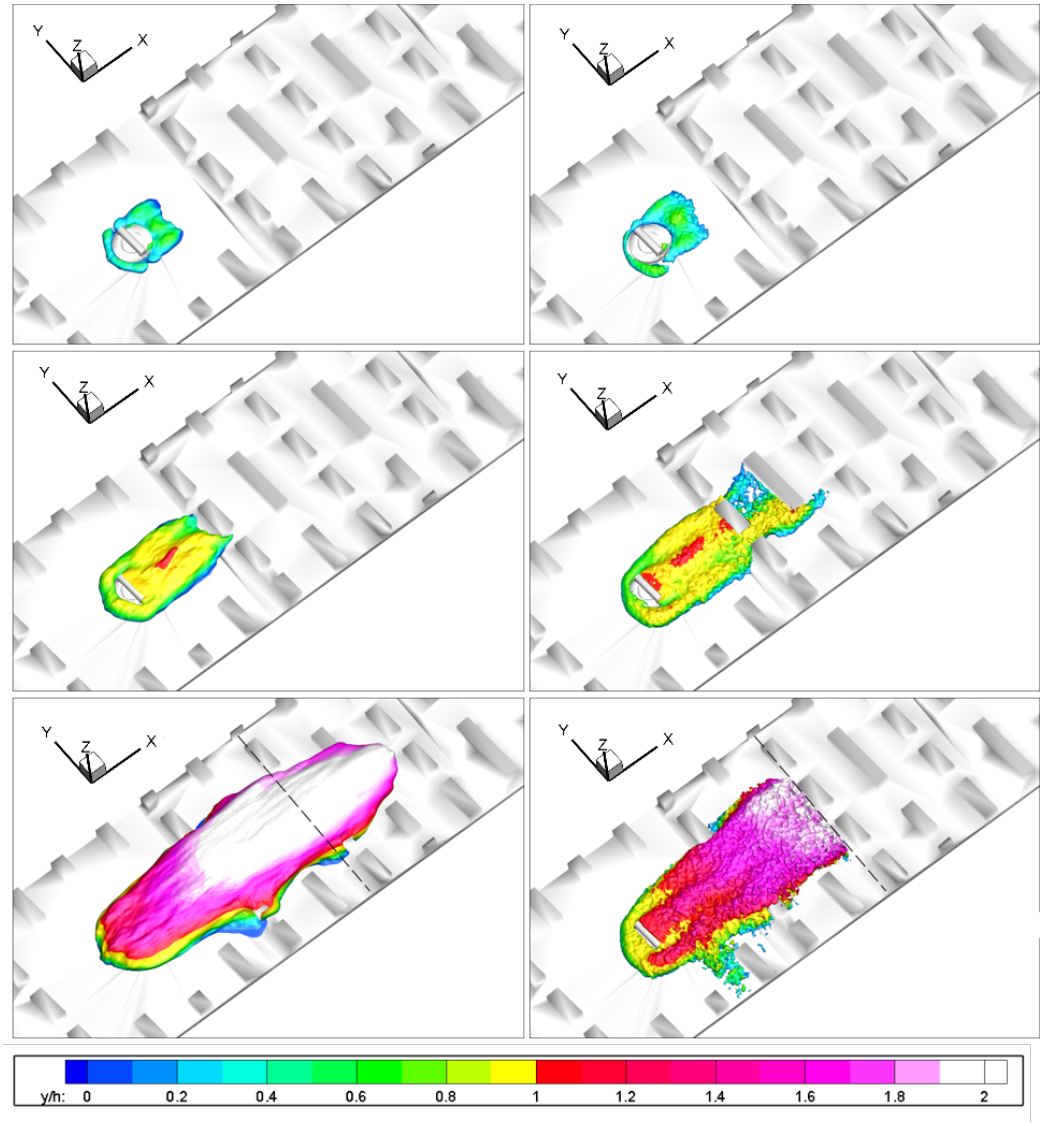

Figure 12: Isosurfaces at 0.20 (top), 0.075 (center), and 0.025 (bottom) of LES simulations (left) and MRC measurements (right), colored by vertical elevation. The red-pink-white colorscale represents elevations above the lower building height, $z/h = 1.0$. Also note the dotted lines in the 0.025 cases represent the extent of the MRC scanned region.

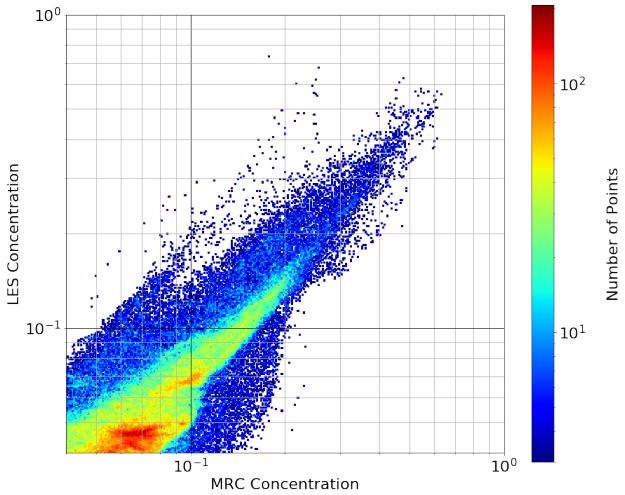

Figure 13: Pointwise concentration comparisons between LES and MRC results within the contaminant plume regions, colored by point density.

surfaces as might be expected. The rapid turbulent mixing of the plume ensures that nearly all the comparison points are below a concentration of 50% with the vast majority below 20% in the field. Table 2 summarizes quantitative metrics from the data presented in Figure 13. In addition to the parameters reported for velocity, Table 2 includes the fractional mean bias (FB), normalized mean-square error (NMSE), normalized absolute difference (NAD), geometric mean (MG), and geometric variance (VG). These metrics are more fully defined and analyzed in the context of urban dispersion in [14].

Figure 14 depicts another comparison between the LES and MRC results showing the spatial distribution of the deviations presented in Figure 13. In each case, all the concentration values have been summed in either the vertical or spanwise locations and contrasted through an arithmetic subtraction. This analysis provides a method to compare the three-dimensional LES and MRC datasets along lines, but does not provide comparison at each spatial location. A manual slice-by-slice comparison has, however, confirmed the trend that the greatest deviation occurs near the injector and along the lower plume edge. Likely, there are subtle differences between the installed geometry of the injector used in the MRC experiments and the idealized design employed in the LES simulation, a fact that would result in concentrations deviations very near the injector and splash plate as shown in Figure 14a.

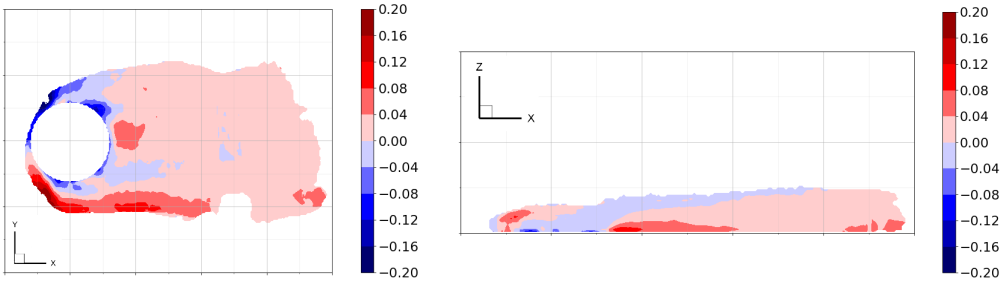

(a) View along z-direction. (b) View along y-direction.

Figure 14: Difference between the mean MRC field and LES field. Positive values (red) represent locations where MRC measurements are greater than LES, while negative values (blue) represent greater LES values.

The bottom region of this same figure also shows an area where the MRC measurements exceed those of the LES. For the bulk of the field, the integrated concentration results are quite similar. Figure 14b shows that the MRC measured higher concentrations downstream of the injection site near the surface, while the LES simulations report higher concentrations at the top of the plume – two observations congruent with the results illustrated in the isosurfaces in Figure 12. These differences are likely due to the choice of parameters used in the LES simulation. Future work will use the MRC dataset to improve the LES simulations.

4. Conclusions

In this work, MRI methods were employed to study a complex flow of chemical contaminant dispersion. Both MRV and MRC techniques were used to collect time-averaged three-component velocity and concentration data for a scaled model of the Jack Rabbit II field test, focusing on the complex flow in the near field for phase 1 tests. The dense gas and phase change of the field tests chlorine release were not modeled, enabling a detailed investigation of a single-phase dispersion event. The scaled flow was also modeled with large-eddy simulations (LES) to provide a dataset for comparison with MR measurements. Despite a complex and three-dimensional flow, the velocity data shows strong qualitative and quantitative agreement between LES simulations and MRV measurements. In some regions, LES predicts greater velocity gradients than MRV results. Concentration results also compared

well between MRC and LES with some differences observed near the injector, likely attributable to subtle differences in the experiment's manufactured geometry compared to the idealized LES domain. As expected, deviation in concentration was also noted near walls and regions of high gradients. Measurement uncertainty was estimated to be ±5% of the bulk mean velocity for the velocity field and ±4% for the concentration field, with principal uncertainty components based on the spatial measurement resolution of 0.8 mm.

5. Acknowledgement

This work was funded by the Defense Threat Reduction Agency (DTRA) through the Research and Development Directorate within the Chem/Bio Information and Analysis Division.

[1] STAR-CCM+. https://www.plm.automation.siemens.com. Library Catalog: www.plm.automation.siemens.com.

[2] 3D Systems Corporation, Rock Hill, SC. *Data Sheet: Accura 60*.

[3] Andrew J. Banko, Filippo Coletti, Christopher J. Elkins, and John K. Eaton. Oscillatory flow in the human airways from the mouth through several bronchial generations. *International Journal of Heat and Fluid Flow*, 61:45–57, October 2016.

[4] Michael Benson, Nicholas Wilde, Alexander Brown, and Christopher Elkins. Detailed magnetic resonance imaging measurements of a contaminant dispersed in an Oklahoma City model. *Atmospheric Environment*, page 117129, 2019.

[5] Michael J. Benson, Christopher J. Elkins, Paul D. Mobley, Marcus T. Alley, and John K. Eaton. Three-dimensional concentration field measurements in a mixing layer using magnetic resonance imaging. *Experiments in Fluids*, 49(1):43–55, October 2009.

[6] Michael J Benson, Bret P Van Poppel, Christopher J Elkins, and Mark Owkes. Three-Dimensional Velocity and Temperature Field Measurements of Internal and External Turbine Blade Features Using Magnetic Resonance Thermometry. *Journal of Turbomachinery*, 141(7):071011, 2019.

[7] Erica M. Cherry, Christopher J. Elkins, and John K. Eaton. Geometric sensitivity of three-dimensional separated flows. *International Journal of Heat and Fluid Flow*, 29(3):803–811, June 2008.

[8] Erica M. Cherry, Angelina M. Padilla, Christopher J. Elkins, and John K. Eaton. Three-dimensional velocity measurements in annular diffuser segments including the effects of upstream strut wakes. *International Journal of Heat and Fluid Flow*, 31(4):569–575, August 2010.

[9] Stanley Corrsin. The isotropic turbulent mixer: Part II. Arbitrary Schmidt number. *AIChE Journal*, 10(6):870–877, 1964. _eprint: https://aiche.onlinelibrary.wiley.com/doi/pdf/10.1002/aic.690100618.

[10] Christopher J. Elkins and Marcus T. Alley. Magnetic resonance velocimetry: applications of magnetic resonance imaging in the measurement of fluid motion. *Experiments in Fluids*, 43(6):823–858, December 2007.

[11] Simon Gant, Jeffrey Weil, Luca Delle Monache, Bryan McKenna, Maria M Garcia, Graham Tickle, Harvey Tucker, James Stewart, Adrian Kelsey, Alison McGillivray, et al. Dense gas dispersion model development and testing for the jack rabbit ii phase 1 chlorine release experiments. *Atmospheric environment*, 192:218–240, 2018.

[12] Steven Hanna. Meteorological Data Recommendations for Input to Dispersion Models applied to Jack Rabbit II Trials, 2018.

[13] Steven Hanna, Rex Britter, Edward Argenta, and Joseph Chang. The jack rabbit chlorine release experiments: Implications of dense gas removal from a depression and downwind concentrations. *Journal of hazardous materials*, 213:406–412, 2012.

[14] Steven Hanna and Joseph Chang. Acceptance criteria for urban dispersion model evaluation. *Meteorology and Atmospheric Physics*, 116(3):133–146, May 2012.

[15] Steven Hanna, Joseph Chang, and Pablo Huq. Observed chlorine concentrations during jack rabbit i and lyme bay field experiments. *Atmospheric environment*, 125:252–256, 2016.

[16] Steven Hanna, Thomas Mazzola, Joseph Chang, and Simon Grant. Overview of Jack Rabbit II (JR II) field experiment and summary of the methods used in the dispersion model comparisons. *Atmospheric environment*, 001:01–02, 2016.

[17] Jane Kay. Chlorine accidents take a big human toll. `https://www.scientificamerican.com/article/chlorine-accidents-take-big-human-toll/`, 2011.

[18] Bryan McKenna, Maria Mallafrè Garcia, Simon Gant, R Batt, M Wardman, H Tucker, G Tickle, H Witlox, M Fernandez, M Harper, et al. Jack rabbit ii 2015 trials: preliminary comparison of the experimental results against drift and phast dispersion model predictions. In *IChemE Hazards 27 Conference, Birmingham, UK*, pages 10–12, 2017.

[19] F. Nicoud and F. Ducros. Subgrid-Scale Stress Modelling Based on the Square of the Velocity Gradient Tensor. *Flow, Turbulence and Combustion*, 62(3):183–200, September 1999.

[20] S. B. Pope. *Turbulent flows*. Cambridge University Press, 2000.

[21] Daniele Schiavazzi, Filippo Coletti, Gianluca Iaccarino, and John K Eaton. A matching pursuit approach to solenoidal filtering of three-dimensional velocity measurements. *Journal of Computational Physics*, 263:206–221, 2014.

[22] Tom Spicer, Audrey Feuvrier, and Shannon B Fox. Transient large-scale chlorine releases in the jack rabbit ii field tests: Rainout source data analysis from video records. *Journal of Loss Prevention in the Process Industries*, 59:35–43, 2019.

[23] Tom Spicer and Derek Miller. Quantifying the mass discharge rate of flashing two phase releases through simple holes to the atmosphere. *Process Safety Progress*, 37(3):382–396, 2018.

[24] Thomas Vik, John Aa Tørnes, and Bjørn Anders P Reif. Simulations of the release and dispersion of chlorine and comparison with the jack rabbit field trials. ffi-rapport 2015/01474. *Forsvarets forskningsinstitutt*, 2015.

[25] Sayuri D. Yapa, John L. DAtri, John M. Schoech, Christopher J. Elkins, and John K. Eaton. Comparison of magnetic resonance concentration measurements in water to temperature measurements in compressible air flows. *Experiments in Fluids*, 55(11):1834, October 2014.